Journal of Power Sources 609 (2024) 234685

Contents lists available at ScienceDirect

Journal of Power Sources

journal homepage: www.elsevier.com/locate/jpowsour

On the formation and properties of amorphous and crystalline $Li_{3-y}Ba_{y/2}OCl$ electrolytes

Junquan Ou [a], Vignyatha Tatagari [a], Ishani Senevirathna [b], Sudarshan Luitel [b], Carlo Segre [b], Leon Shaw [a,*], M. Helena Braga [c]

[a] Department of Mechanical, Materials and Aerospace Engineering, USA
[b] Department of Physics, Illinois Institute of Technology, Chicago, IL, 60616, USA
[c] Engineering Physics Department, Engineering Faculty, University of Porto, 4200-465, Porto, Portugal

HIGHLIGHTS

- Hydrothermal synthesis of amorphous and crystalline $Li_{3-y}Ba_{y/2}OCl$ electrolytes.
- First use of vacuum to accelerate vapor release in hydrothermal synthesis.
- Enhancing the formation of amorphous $Li_{3-y}Ba_{y/2}OCl$ via vacuum-assisted drying.
- Amorphous $Li_{2.99}Ba_{0.005}OCl$ exhibits 7.65×10^{-3} S/cm ionic conductivity at RT.

ARTICLE INFO

Keywords:
Solid-state electrolytes
Lithium oxychloride
Ionic conductivity
Electrochemical window
Solid-state batteries

ABSTRACT

All-solid-state batteries (ASSBs) have potential to provide higher specific energy, higher power, and longer cycle life than Li-ion batteries (LIBs) for continuously increasing demands of high-performance rechargeable batteries with intrinsic safety. However, one of the barriers for successful design and fabrication of ASSBs is the lack of solid-state electrolytes (SSEs) that can meet multi-functional requirements for ASSBs. To address this issue, the present study investigates hydrothermal synthesis of amorphous and crystalline Ba-doped Li_3OCl solid electrolytes and develops the understanding of the relationships between the synthesis conditions and electrochemical properties of the products. It is shown that the formation of an amorphous/crystalline Ba-doped Li_3OCl mixture with little hydroxide impurities depends strongly on the hydrothermal reaction temperature, drying temperature, Ba concentration, and rate of removing OH^- and H^+ ions as steam from water solvated Ba-doped Li_3OCl. The key to generate amorphous Li_3OCl-based electrolytes with high ionic conductivities (7.65×10^{-3} S/cm) at room temperature is to create non-equilibrium synthesis conditions such as the one identified in this study. The understanding developed in this study will offer critical guidelines for synthesizing amorphous and crystalline Li_3OCl-based electrolytes with superior electrochemical properties for ASSBs reliably and reproducibly in the near future.

1. Introduction

The fundamentally safe nature and the potential of higher energy density of all-solid-state batteries (ASSBs) than Li-ion batteries (LIBs) have spurred enormous research activities worldwide for the last 20 years [1–4]. One of the challenges for ASSBs is the lack of solid-state electrolytes (SSEs) that offer the solutions to all the challenges faced by ASSBs. For instance, polyethylene oxide (PEO)-based polymer electrolytes have the advantages of outstanding film-forming ability, high flexibility for good physical contact with electrodes, and low processing cost [3]. However, they have low ionic conductivity at RT (10^{-5} to 10^{-8} S/cm) and inferior electrochemical window [2,3]. In contrast, oxide-based electrolytes, such as the garnet-type cubic $Li_7La_3Zr_2O_{12}$ (LLZO) and their doped variants, possess high ionic conductivity ($\sim 10^{-4}$ S/cm) and excellent stability against Li metal and cathodes, but they have high interfacial resistance due to their rigid ceramic nature and poor physical contact between the electrode and electrolyte [2–4]. Sulfide-based electrolytes, such as $Li_7P_3S_{11}$, have very high ionic

* Corresponding author.
E-mail address: lshaw2@iit.edu (L. Shaw).

https://doi.org/10.1016/j.jpowsour.2024.234685
Received 11 March 2024; Received in revised form 19 April 2024; Accepted 6 May 2024

conductivities, but are not electrochemically stable with many cathodes and even react with cathode materials during high-temperature or high-pressure processing [5]. Reactions between sulfide-based electrolytes (e.g., $Li_{10}GeP_2S_{12}$) with acetylene black conductive additives have also been reported when charging above 4.5 V vs. Li^+/Li) [6]. Costings, such as $LiNbO_3$ [7], Li_2O–SiO_2 glass [8], $LiAlO_2$ [9], Li_3PO_4 [10], Li_2MnO_4 [11], $Li_4Ti_5O_{12}$ [12] and $LiTaO_3$ [13], have all been shown to have beneficial effects in suppressing side reactions between the cathode and sulfide-based electrolytes, thereby improving their interfacial stability. In spite of these advancements, further improvements in SSEs are still required for practical applications.

Recently, Braga and her team working with Prof. John Goodenough, the Nobel laureate in Chemistry in 2019, have reported a new type of Li-glass electrolytes with compositions of $Li_{2.99}Ba_{0.005}O_{1+x}Cl_{1-2x}$ ($0 < x < 1$) [14,15]. The new Li-glass electrolytes are reported to possess ultra-high ionic conductivity at room temperature (RT) ($>10^{-2}$ S/cm which is similar to that of the conventional liquid carbonate electrolytes), have wide electrochemical windows, are stable with Li and Na metals, and exhibit resistance to oxidation up to 8 V (vs. Li^+/Li) [15–21]. These unusual properties derived from one SSE represents a major breakthrough in SSE technology. However, many other researchers [22–26] working on Li_3OCl-based electrolytes often obtain crystalline anti-perovskite phases rather than glassy phases, indicating difficulty in obtaining glassy Li_3OCl-based electrolytes. Furthermore, crystalline Li_3OCl-based electrolytes typically have lower ionic conductivities (8.9×10^{-6} – 1.9×10^{-3} S/cm at RT) than Li-glass electrolytes [22–27]. Thus, there is a critical need to study how to obtain Li_3OCl-based Li-glass electrolytes consistently with high ionic conductivities and investigate the effects of synthesis conditions on the electrochemical properties of Li-glass electrolytes obtained under different conditions.

With the aforementioned challenge in mind, this study is initiated and focuses on hydrothermal synthesis of amorphous and crystalline $Li_{3-y}Ba_{y/2}OCl$ ($0.01 < y < 0.04$) electrolytes. Ba-dopant has been chosen in this investigation because a previous study [14] has revealed that Ba^{2+} ions with a larger ionic radius than Mg^{2+} and Ca^{2+} ions lead to a lower glass transition temperature for the doped Li-glass electrolyte. A lower glass transition temperature transition enables faster ionic transport at room temperature, confirming that Ba^{2+} is the most effective dopant among the various dopants investigated previously [14]. Hydrothermal synthesis is chosen for the focused investigation here because Li-glass electrolytes reported by Braga's group are synthesized using this method [14,15]. However, a recent study reveals the presence of a large amount of hydroxides in the Li_3OCl product using the same hydrothermal method [26]. The inconsistent results from different researchers underscore the necessity of further studies to identify proper conditions in forming amorphous Li_3OCl-based electrolytes with little or no hydroxide impurities via hydrothermal synthesis and develop understanding of the relationship between the electrochemical properties and synthesis conditions of Li_3OCl-based electrolytes. This understanding will offer crucial guidelines for synthesizing amorphous and crystalline Li_3OCl-based electrolytes with superior electrochemical properties for ASSBs reliably and reproducibly in the near future.

2. Experimental

2.1. Synthesis of electrolyte powder

The Li-glass electrolytes, $Li_{3-y}Ba_{y/2}OCl$ ($0.01 < y < 0.04$), were synthesized from high-purity commercial precursors: LiCl (purity > 99.98 %, Sigma), Li(OH) (purity > 98 %, Sigma), and $Ba(OH)_2 \cdot 8H_2O$ (purity > 98 %, Sigma). The precursors were mixed in an appropriate ratio and dispersed in deionized water in a PTFE autoclave. After vibrating the slurry in an ultrasonic bath for 20 min to disperse the powder mixture, the autoclave was heated to 150 °C for at least 2 h to dissolve all the raw materials. Then the transparent solution was subjected to hydrothermal reactions in an autoclave equipped with a pressure release valve, operating at 250 °C for at least 3 h. Following the hydrothermal reactions, the pressure release valve was opened to remove water steam rapidly at 250 °C or at other high temperatures (to be specified later). For some synthesis experiments, a vacuum pump connected to the autoclave was turned on during holding at 250°C and cooling of the autoclave to room temperature (RT) to remove any residual moisture in the product. To accomplish different drying conditions, a custom-made autoclave was constructed (see Fig. S1 in Supplemental Information). Briefly, a pressure release valve was connected to the cap of the autoclave. Once hydrothermal synthesis reached the pre-determined reaction time, the pressure release valve could be opened manually, and the steam could be released to either the ambient air or a vacuum pump controlled via a three-way valve. The Li-glass powder product after synthesis was taken out from the autoclave at RT inside an Ar-filled glovebox ($H_2O < 0.1$ ppm, $O_2 < 1$ ppm, MBRUAN UNIlab) and kept inside the glovebox for subsequent use and analysis.

2.2. Material characterization

The X-ray diffraction (XRD) patterns of the products were collected in the 2θ range of 15–80° at a scan rate of 0.01° per second using a Bruker D2 Phaser Diffractometer with Cu *K*α radiation (λ = 1.54056 Å). To avoid reactions with moisture during the XRD data collection, sample powder was sealed with a Kapton tape or inside an airtight, X-ray transparent, dome-type specimen holder from Bruker. The differential scanning calorimetry (DSC) analysis was conducted using the Setsys 16/18 DTA/DSC from Setaram to determine the glass transition temperature of the amorphous electrolyte, the melting point of the crystalline electrolyte, and the melting point of hydroxide phases if present. The DSC analyses were performed from 30 °C to 300 °C in the first cycle and 30 °C–330 °C in the second cycle inside an alumina crucible under an argon atmosphere with a heating and cooling rate of 5°C/min.

2.3. Electrochemical measurement

250 mg of Li-glass powder was first cold pressed at 200 MPa and then heated to 100 °C to form a pellet in a steel die with a garolite sleeve. The impedance of the pellet was measured via electrochemical impedance spectroscopy (EIS, Gamry INTERFACE 1010E) over a frequency range of 1 Hz–2 MHz with an applied AC perturbation signal of 30 mV. EIS data analysis and equivalent circuit fitting for calculating the electrical conductivity were performed using Gamry Echem Analyst. DC polarization was conducted with a voltage of 5 V right after the EIS measurement. The cyclic voltammetry (CV) was conducted using Gamry INTERFACE 1010E with a semi-blocking cell having a stainless steel/solid-state electrolyte/Li chip/stainless steel (SS/SSE/Li/SS) setup to obtain the electrochemical window. The test was performed at RT with a scanning rate of 1 mV/s within the range of −0.5 V–6.0 V (vs. Li^+/Li).

3. Results and discussion

3.1. $Li_{2.99}Ba_{0.005}OCl$ synthesis and hydroxide impurities

The products from the reactions between LiOH and LiCl depend on the synthesis condition and the starting material compositions. Several products and possible reactions have been reported as shown below [14,22,23].

$$2LiOH + LiCl = Li_3OCl + H_2O \quad (1)$$

$$3LiOH + LiCl = Li_4Cl(OH)_3 \quad (2)$$

$$LiOH + LiCl = Li_2(OH)Cl \quad (3)$$

$$2LiOH + 3LiCl = Li_5(OH)_2Cl_3 \quad (4)$$

Fig. 1 is the XRD pattern of a $Li_{2.99}Ba_{0.005}OCl$ powder product

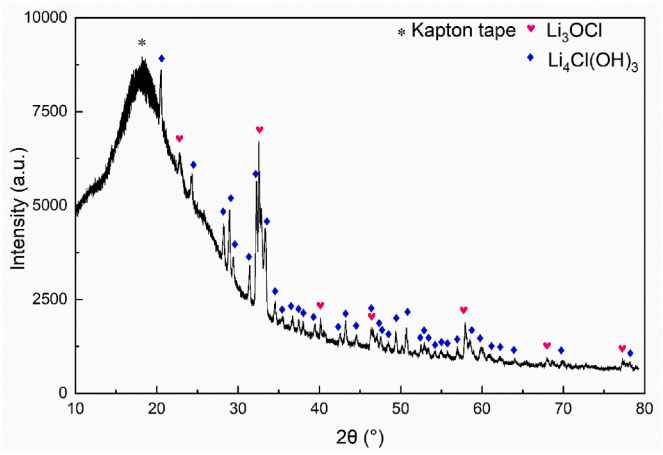

Fig. 1. XRD pattern of a $Li_{2.99}Ba_{0.005}OCl$ powder product which contains hydroxides. See the text for the discussion of the synthesis condition.

synthesized via complete dissolution of all raw materials in deionized water at 150°C, followed by heating to 225 °C and maintained at that temperature for 24 h. Subsequently, the pressure release valve was opened to allow water vapor release from the autoclave at 225 °C for 1 h. No water vapor was observed after 1h opening of the pressure release valve. Upon closure of the pressure release valve, the autoclave was removed from the heating sand bath and allowed to cool to near room temperature (RT). After cooling to RT the powder product was taken out from the autoclave inside an argon-filled glovebox. As shown in Fig. 1, the final product from this process is a mixture of $Li_{2.99}Ba_{0.005}OCl$ and $Li_4Cl(OH)_3$ hydroxide. Clearly, the synthesis condition used in this experiment fails to expeditiously and thoroughly remove residual moisture from the autoclave, thereby promoting the formation of $Li_4Cl(OH)_3$ impurity as shown in Reaction (2), along with the formation of $Li_{2.99}Ba_{0.005}OCl$ which requires complete removal of any moisture as indicated by Reaction (1).

Fig. 2 shows the XRD patterns of two other $Li_{2.99}Ba_{0.005}OCl$ powder products that were generated with hydrothermal reactions at 250 °C for 24 h, followed by releasing the pressure valve to remove water vapor rapidly at 250 °C. During the vapor releasing process, a vacuum pump connected to the autoclave was turned on for 24 h to help remove any residual moisture and prevent the formation of hydroxides. For one group of powder the drying temperature was maintained at 250°C for 24 h, whereas for the second group of powder the drying temperature was reduced to 210°C after holding at 250°C for 30 min. Then, the autoclaves were allowed to cool and transferred to an Ar-filled glovebox ($H_2O < 0.1$ ppm, $O_2 < 1$ ppm) after the temperature were dropped to

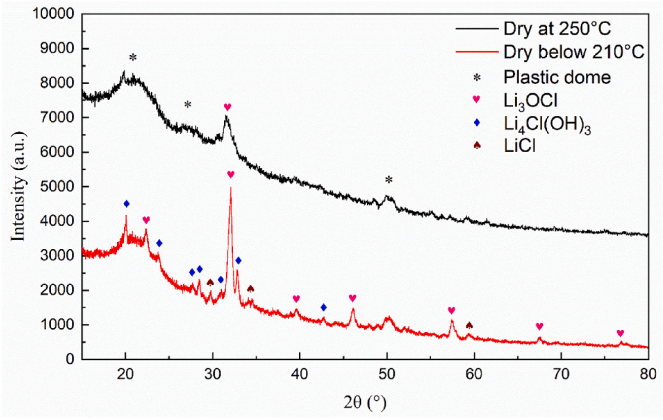

Fig. 2. X-ray diffraction patterns of $Li_{2.99}Ba_{0.005}OCl$ drying at different temperatures.

150 °C. As shown in Fig. 2, the sample dried at 250°C has crystalline $Li_{2.99}Ba_{0.005}OCl$ with little hydroxide, whereas the sample dried at 210°C still contains a substantial amount of $Li_4Cl(OH)_3$ hydroxide and unreacted LiCl. Note that the broad peaks at $2\theta = 21°$, 27° and 51° originate from the airtight plastic sample holder, whereas the main characteristic diffraction peaks appear at $2\theta = 22.74°$, 32.38°, 39.93°, 46.44°, and 57.75°, corresponding to Li_3OCl anti-perovskite structure with O^{2-} ions located at the center of the unit cell, Cl^- ions at the eight cube vertices, and Li^+ ions at the six face centers of the unit cell [28]. These experiments reveal that complete drying at 250°C is essential to avoid the formation of hydroxides. Drying at 210°C is not sufficient to prevent the formation of $Li_4Cl(OH)_3$ hydroxide. As will be shown later, the melting temperature of $Li_4Cl(OH)_3$ hydroxide is at 215°C. Thus, it is proposed that drying above 215°C at the liquid state of $Li_4Cl(OH)_3$ under a dynamic vacuum condition (with a mechanical pump on) may result in gradual decomposition of $Li_4Cl(OH)_3$, thereby minimizing the formation of $Li_4Cl(OH)_3$. Hydroxide impurities have lower conductivities than Li_3OCl [29] and thus the hydrothermal synthesis conditions identified in this study to form $Li_{2.99}Ba_{0.005}OCl$ with little or no hydroxide impurities are significant.

It should be pointed out that the broad peak at 32° for $Li_{2.99}Ba_{0.005}OCl$ dried at 250°C is indicative of crystalline $Li_{2.99}Ba_{0.005}OCl$ with nanograins. The unsymmetric shape of the broad peak suggests the presence of a minute amount of $Li_4Cl(OH)_3$ hydroxide, leading to merging of the peaks from $Li_{2.99}Ba_{0.005}OCl$ and $Li_4Cl(OH)_3$. The absence of the other $Li_{2.99}Ba_{0.005}OCl$ crystalline peaks (such as those at $2\theta = 22.74°$, 39.93°, 46.44°, and 57.75°) for the sample dried at 250°C indicates that the quantity of crystalline $Li_{2.99}Ba_{0.005}OCl$ is low in this sample, i.e., a significant amount of $Li_{2.99}Ba_{0.005}OCl$ is in the amorphous state, which will be discussed below.

3.2. *Formation of amorphous and crystalline $Li_{2.99}Ba_{0.005}OCl$ electrolytes*

Since it is difficult to detect amorphous phases using XRD, differential scanning calorimetry is utilized to study whether there is an amorphous phase in the $Li_{2.99}Ba_{0.005}OCl$ product synthesized and dried at 250°C. As shown in Fig. 3a (the first DSC scan), a distinct glass transition temperature of the amorphous $Li_{2.99}Ba_{0.005}OCl$ is observed at approximately 100 °C, along with the melting point of the hydroxide phase (T_{m1}) at 215 °C and the melting point of the crystalline $Li_{2.99}Ba_{0.005}OCl$ (T_{m2}) at 268 °C, similar to those reported in Refs. 14, 22 and 26. The solidification temperature of crystalline $Li_{2.99}Ba_{0.005}OCl$ (T_s) was observed at 240 °C in the cooling curve. In the second scan (Fig. 3b), T_{m1}, T_{m2} and T_s are still present, but T_g has disappeared, suggesting that melting and re-solidification with a heating/cooling rate at 5 °C/min will not lead to the formation of amorphous $Li_{2.99}Ba_{0.005}OCl$. Additionally, the T_{m1} peak becomes smaller in the second scan, revealing that some hydroxide has decomposed after heating above its melting temperature – a phenomenon consistent with our previous hypothesis that drying at 250°C in the hydrothermal synthesis process may result in decomposition of $Li_4Cl(OH)_3$ hydroxide and thus minimize the formation of $Li_4Cl(OH)_3$ hydroxide. The co-presence of amorphous and crystalline Li_3OCl phases along with a tiny amount of hydroxide in the hydrothermally synthesized sample is consistent with the previous studies [14,26]. Furthermore, the measured T_g, T_{m1} and T_{m2} values in this study are very close to those reported by Braga's group [14] and Khakpour's team [26].

To corroborate the DSC results independently, the $Li_{2.99}Ba_{0.005}OCl$ product synthesized and dried at 250°C was analyzed using XRD at the as-synthesized condition and after melting and re-solidification condition. In this set of XRD experiments (Fig. 4), both samples were sealed with a Kapton tape during the data collection. Because Kapton sealing is not as good as the sealing provided by the airtight, dome-type specimen holder from Bruker, some $Li_{2.99}Ba_{0.005}OCl$ has picked up minute moisture and changes to $Li_4Cl(OH)_3$ and $Li_2(OH)Cl$ hydroxides during the XRD data collection even though the sample before melting in Fig. 4 is

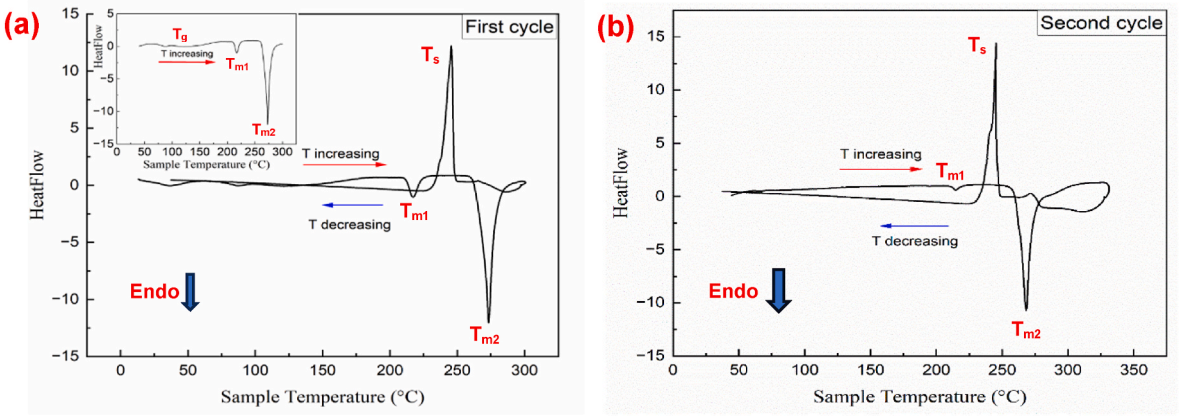

Fig. 3. Differential scanning calorimetry of the $Li_{2.99}Ba_{0.005}OCl$ synthesized and dried 250°C at a scanning rate of 5 °C min^{-1} for two heating/cooling cycles: (a) first scan and (b) second scan. The insert in (a) is the heating curve of the first scan.

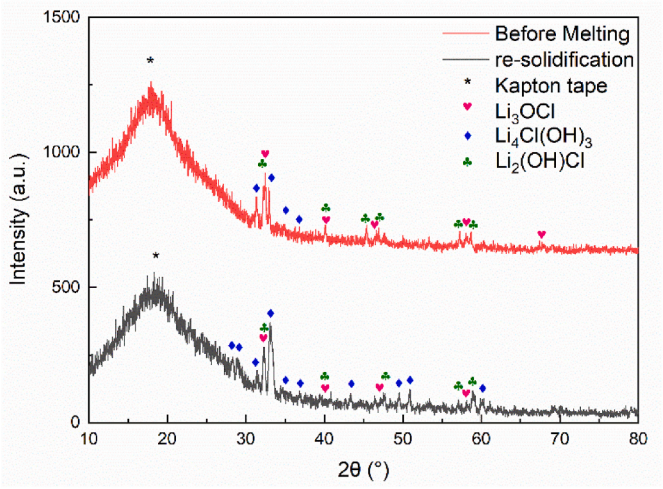

Fig. 4. X-ray diffraction patterns of $Li_{2.99}Ba_{0.005}OCl$ synthesized and dried at 250°C: (a) at the as-synthesized condition and (b) after melting and re-solidification. Both samples were sealed using a Kapton tape during XRD data collection.

identical as the one in Fig. 2 dried at 250°C. In spite of this complication, a comparison between the as-synthesized sample and the melt and re-solidified sample reveals the intensity increase of the crystalline $Li_{2.99}Ba_{0.005}OCl$ peaks after melting and re-solidification. This finding serves to reinforce the conclusions drawn from the DSC analysis, i.e., melting and re-solidification at a heating/cooling rate of 5 °C/min cannot lead to formation of amorphous $Li_{2.99}Ba_{0.005}OCl$. Note that the $Li_{2.99}Ba_{0.005}OCl$ sample in Fig. 4 before melting has sharp $Li_{2.99}Ba_{0.005}OCl$ peaks, whereas the sample in Fig. 2 dried at 250°C has only one broad peak at 32°. As mentioned before, the broad peak at 32° for the sample in Fig. 2 is due to the formation of $Li_{2.99}Ba_{0.005}OCl$ with nanograins. The sharp peaks of the sample in Fig. 4 before melting are indicative of $Li_{2.99}Ba_{0.005}OCl$ with grain sizes significantly larger than 100 nm. The difference in their grain sizes is likely attributed to their different hydrothermal reaction times (i.e., 2 days for the sample in Figs. 4 and 7 days for the sample in Fig. 2). The effects of the hydrothermal reaction time are outside the scope of this study, but should be the area of investigation in the near future.

To further explore the possibility of forming amorphous $Li_{2.99}Ba_{0.005}OCl$ phase via fast cooling, we have designed a special experiment by sealing the $Li_{2.99}Ba_{0.005}OCl$ powder obtained from hydrothermal synthesis in an argon-filled stainless steel tube and heating this tube at 300°C for 35 min, followed by quenching this tube in cold water (15°C). The steel tube temperature reaches 15°C in 4 min, resulting in an average cooling rate > 70 °C/min. The XRD patterns of the $Li_{2.99}Ba_{0.005}OCl$ powders before melting and after quenching are compared in Fig. 5. Interestingly, the results are the same as those found from the DSC and XRD analyses in Figs. 3 and 4, respectively. That is, melting at 300°C followed by cooling at 70 °C/min has reduced the hydroxide content and increased the peak intensity of the crystalline $Li_{2.99}Ba_{0.005}OCl$ phase.

Taking all the results of this study together, it can be concluded that amorphous $Li_{2.99}Ba_{0.005}OCl$ cannot be formed by melting and re-solidification at heating/cooling rates of 5 °C/min and 70 °C/min. Instead, amorphous $Li_{2.99}Ba_{0.005}OCl$ phase can be formed via reactions between LiCl and LiOH in the presence of water and rapid removal of water at high temperatures, followed by drying at temperature at about 250°C. A possible mechanism via water solvation to form amorphous Li_3OCl phase under the aforementioned conditions has been proposed by Braga's group [15]. Our results are in good accordance with the previously proposed mechanism.

It should be pointed out that Khakpour's team [26] used 235°C for hydrothermal reactions and drying also obtained a mixture of amorphous and crystalline Li_3OCl but with more hydroxides in comparison with hydrothermal reactions and drying at 250°C (Fig. 2). Thus, hydrothermal reactions and drying at 250°C have advantages of little hydroxide(s) over hydrothermal reactions and drying at 235°C [26], 225°C, or 210°C (this study). Interestingly, Khakpour's team [26] has reported that an amorphous hump in the range of 2θ = 31°–37° appears

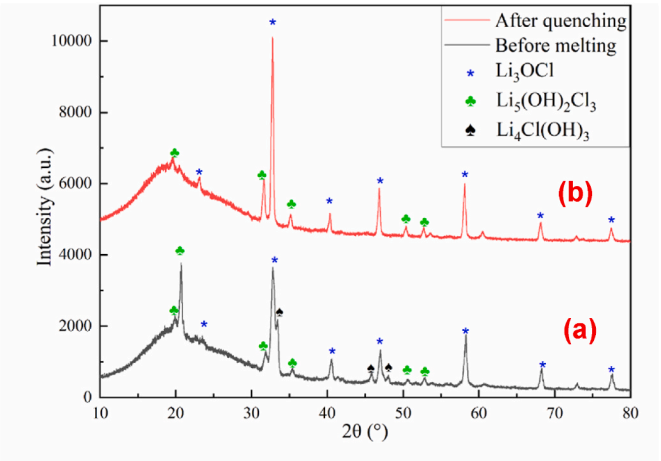

Fig. 5. X-ray diffraction patterns of $Li_{2.99}Ba_{0.005}OCl$: (a) before melting and (b) after melting at 300°C and cooling at 70 °C/min.

along with substantial decrease in the intensities of crystalline Li_3OCl peaks after heat treatment, showing that amorphous Li_3OCl can be formed via heat treatment after hydrothermal synthesis. However, heat treatment conditions were not described [26].

3.3. Electrochemical properties of $Li_{2.99}Ba_{0.005}OCl$ electrolytes

The impedance of $Li_{2.99}Ba_{0.005}OCl$ synthesized and dried at 250°C has been determined using EIS. As shown in Fig. 6, the Nyquist plot of the SS/Li-glass pellet/SS cell at RT show a depressed semicircle in the high frequency region followed by a straight line in the low frequency region. An equivalent circuit, R(Q(RW)) shown in Fig. 6, is used to fit the impedance spectrum. It is known that the intercept of the semicircle with the real axis at the highest frequency typically represents R_{bulk} derived from the resistance to Li-ion transport inside solid electrolyte particles, whereas R_{gb} determined from the semicircle is normally attributed to resistance of Li-ion diffusion via grain boundaries and/or particle interfaces [30,31]. Based on the R(Q(RW)) fitting result, the electrical conductivities, σ_{bulk} and σ_{gb}, are calculated from R_{bulk} and R_{gb}, respectively, with the aid of the following equation:

$$\sigma = \frac{L}{RA} \tag{5}$$

where σ, L, R and A represent the conductivity, thickness, resistance and area of the Li-glass pellet, respectively. The bulk conductivity of Li-glass, σ_{bulk}, at room temperature is determined to be 7.65×10^{-3} S/cm, and the grain boundary/interface conductivity, σ_{gb}, is about 2.74×10^{-7} S/cm. The total conductivity of the Li-glass pellet including the contributions of Li-ion transport via the grain interior, grain boundaries and particle interfaces, σ_{total}, is determined to be 2.74×10^{-7} S/cm, dominated by the small conductivity of σ_{gb}.

To separate the electronic and ionic conductivities, a DC polarization experiment was conducted. As determined from Fig. 7a, the total electrical conductivity at the 1st second of the DC polarization experiment is 7.5×10^{-7} S/cm, whereas the electronic conductivity is approximately 1.5×10^{-7} S/cm determined at 1800 s of the DC polarization experiment. As such, the electrical conductivity of the Li-glass pellet is mainly dictated by the ionic conductivity which is about 6.0×10^{-7} S/cm, close to σ_{total} determined from EIS measurement.

The electrochemical window of $Li_{2.99}Ba_{0.005}OCl$ synthesized and dried at 250°C has been determined via cyclic voltammetry. The CV curve of a semi-blocking SS/Li-glass/Li/SS cell in the range of 0–6 V vs. Li^+/Li is shown in Fig. 7b. There is a small oxidation peak detected at about 5.3 V, but no corresponding reduction peak is observed. Notably, there is no reduction peak at 0 V, indicating that the Li-glass electrolyte is stable with the lithium anode, which is consistent with the previous measurement [14,15]. A recent density functional theory (DFT) calculation discloses that amorphous Li_3OCl is stable against Li metal electrode, whereas crystalline Li_3OCl is not [32]. According to Ref. 32, the reason for the stability of amorphous Li_3OCl against Li metal is that amorphous Li_3OCl contains oxygen vacancies, thereby diminishing the number of oxygen atoms available for bonding with Li and thus enhancing its stability against Li metal. In addition, the presence of oxygen-oxygen pairs in the amorphous structure further limits the available oxygen for lithium bonding, bolstering its stability against lithium metal [32]. Thus, the stability of $Li_{2.99}Ba_{0.005}OCl$ synthesized in this study against Li metal electrode is attributed to the presence of amorphous $Li_{2.99}Ba_{0.005}OCl$ phase. The wide electrochemical window (from 0.0 to 5.3 V vs. Li^+/Li) of Li-glass synthesized via hydrothermal processing offers a great potential for making ASSBs with high energy densities derived from Li metal anodes and 5V cathodes.

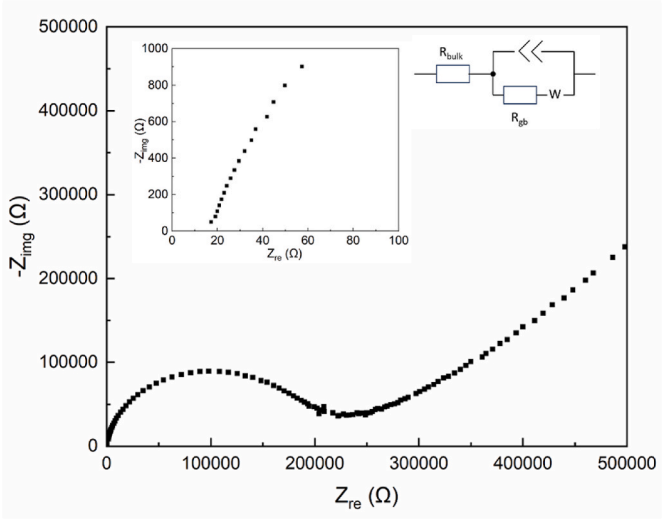

Fig. 6. Nyquist plot of the SS/Li-glass/SS cell measured at RT with a compression stress of 50 MPa. The insert shows the detail of the highest frequency region and the equivalent circuit used for curve fitting.

3.4. Properties of $Li_{3-y}Ba_{y/2}OCl$ with different Ba concentrations

The influence of the concentration of Ba ion doping has been systematically examined. In contrast to the synthesis of the amorphous-phase-dominated $Li_{2.99}Ba_{0.005}OCl$ with a vacuum pump drying at 250°C, the procedure for synthesizing Li_3OCl with different Ba concentrations did not involve a vacuum-pump-assisted drying process. Consequently, the resultant products are mainly composed of Ba^{2+}-doped crystalline Li_3OCl along with the formation of $Li_4Cl(OH)_3$ hydroxide (Fig. 8a). Based on EIS measurements and using R(Q(RW)) equivalent circuit, the conductivities of $Li_{3-y}Ba_{y/2}OCl$ ($0.01 < y < 0.04$) with different Ba concentrations at 100°C are summarized in Table 1. $Li_{2.99}Ba_{0.005}OCl$ is found to have the lowest bulk conductivity, σ_{bulk} (5.00×10^{-5} S cm^{-1}), followed by $Li_{2.98}Ba_{0.01}OCl$ and finally $Li_{2.96}Ba_{0.02}OCl$. This trend is consistent with the expectation of gradually increased vacancy concentrations and thus faster Li-ion diffusion induced by a gradual increase in the Ba^{2+} concentration. In contrast, $Li_{2.99}Ba_{0.005}OCl$ has the highest σ_{gb}, followed by $Li_{2.98}Ba_{0.01}OCl$ and finally $Li_{2.96}Ba_{0.02}OCl$. This σ_{gb} trend is completely opposite to the σ_{bulk} trend, and likely due to the increased hydroxide concentration as Ba concentration increases (Fig. 8b). Hydroxide impurities are present at the particle interface and thus lead to reduced grain boundary/interface conductivities.

It should be pointed out that $Li_{2.99}Ba_{0.005}OCl$ synthesized with vacuum-pump-assisted drying at 250°C has a much higher bulk conductivity (7.65×10^{-3} S/cm) at RT than $Li_{2.99}Ba_{0.005}OCl$ synthesized without vacuum-pump-assisted drying at 250°C (only 5.00×10^{-5} S/cm at 100°C). The precise reason for such a huge difference is not clear at this stage, but it may be related to different degrees of atomic randomness of the amorphous $Li_{2.99}Ba_{0.005}OCl$ phase. With a vacuum pump on during holding and drying at 250°C in hydrothermal synthesis, the removal of OH^- and H^+ ions from water-solvated $Li_{2.99}Ba_{0.005}OCl$ is faster and deviates more from the equilibrium condition, thereby creating a higher degree of atomic randomness of the amorphous $Li_{2.99}Ba_{0.005}OCl$ phase which could have a much higher ionic conductivity. Whether this hypothesis is correct or not requires additional investigation in the future.

To confirm that the advantage of removing OH^- and H^+ ions from water-solvated $Li_{2.99}Ba_{0.005}OCl$ with assistance of a vacuum pump is present in other Ba-doped Li_3OCl as well, $Li_{2.98}Ba_{0.01}OCl$ powder is synthesized and dried at 250°C with a vacuum pump. The EIS measurements reveal that both bulk and interface conductivities are higher when drying is assisted with a vacuum pump. Specifically, $Li_{2.98}Ba_{0.01}OCl$ pellets dried at 250°C with assistance of a vacuum pump offer a bulk conductivity of 7.51×10^{-4} S/cm and an interface conductivity of 6.72×10^{-5} S/cm at 100°C. These two conductivities are

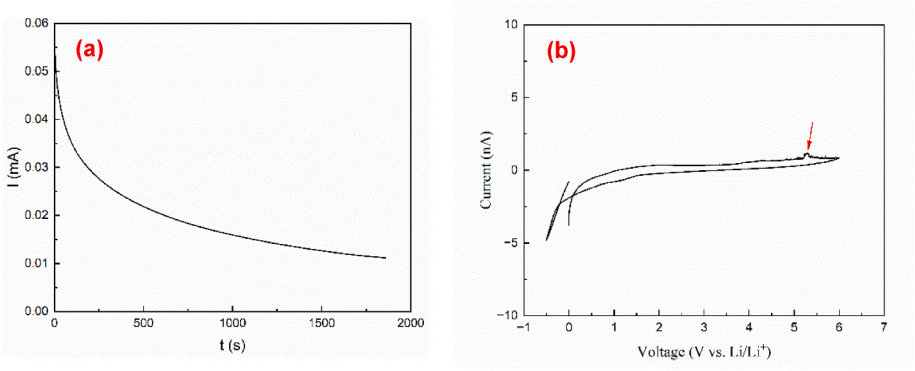

Fig. 7. (a) DC polarization curve of the Li-glass pellet at RT, and (b) cyclic voltammetry curve of the SS/Li-glass/Li/SS semi-blocking cell.

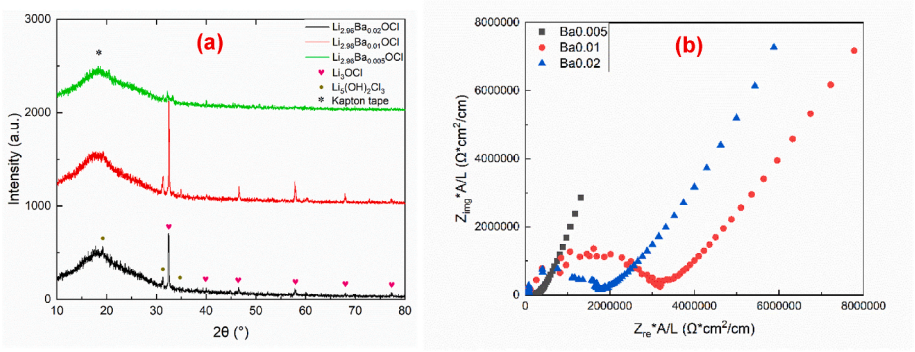

Fig. 8. (a) X-ray diffraction patterns of Li_3OCl with different concentrations of Ba^{2+} dopant, and (b) Nyquist plots of the SS/Li-glass/SS cells measured at 100 °C with a compressive stress of 100 MPa.

Table 1
Conductivities of Li_3OCl with different Ba concentrations derived from EIS measurement.

Sample ID	Pressure	Temp	σ_{bulk} (S/cm)	σ_{inter} (S/cm)
$Li_{2.99}Ba_{0.005}OCl$	40 MPa	100 °C	5.00×10^{-5}	4.28×10^{-6}
$Li_{2.98}Ba_{0.01}OCl$	50 MPa	100 °C	5.16×10^{-5}	3.59×10^{-7}
$Li_{2.96}Ba_{0.02}OCl$	50 MPa	100 °C	5.21×10^{-5}	5.90×10^{-7}

either one or two orders of magnitude higher than the corresponding values shown in Table 1 where the conductivities of $Li_{2.98}Ba_{0.01}OCl$ pellets dried at 250°C but without assistance of a vacuum pump are listed, confirming that the significant improvements in conductivities achieved via drying at 250°C with assistance of a vacuum pump are applicable to Li_3OCl with different Ba concentrations.

Before closing, it is worth emphasizing that amorphous $Li_{3-y}Ba_{y/2}OCl$ ($0.01 < y < 0.04$) electrolyte can be formed via hydrothermal synthesis, as demonstrated in this study. However, the products and their ionic conductivities are very sensitive to hydrothermal synthesis temperature, drying conditions and the Ba dopant concentration. Even with both the hydrothermal reaction temperature and drying temperature being set at 250°C, the presence of hydroxide impurities in and the ionic conductivities of the final $Li_{3-y}Ba_{y/2}OCl$ electrolytes vary substantially with the removing rate of OH^- and H^+ ions from water-solvated $Li_{3-y}Ba_{y/2}OCl$ at 250°C. Rapidly removing OH^- and H^+ ions as steam at 250°C without the assistance of a vacuum pump results in an amorphous/crystalline $Li_{3-y}Ba_{y/2}OCl$ mixture along with the presence of significant hydroxides and the final electrolyte has low bulk and interface conductivities. In contrast, if rapidly removing OH^- and H^+ ions as water steam at 250°C is assisted with a vacuum pump, an amorphous/crystalline $Li_{3-y}Ba_{y/2}OCl$ mixture is also the final product but with little hydroxides. More importantly, the bulk and interface conductivities of the final product is high. These phenomena suggest that rapidly removing OH^- and H^+ ions as steam from water-solvated $Li_{3-y}Ba_{y/2}OCl$ at 250°C with no assistance of a vacuum pump has created a non-equilibrium condition to allow some $Li_{3-y}Ba_{y/2}OCl$ to form amorphous rather than crystalline phase. With the assistance of a vacuum pump the rate of removing OH^- and H^+ ions as steam at 250°C becomes even faster and thus the phase transformation condition is deviated even more from the equilibrium condition, thereby creating amorphous $Li_{3-y}Ba_{y/2}OCl$ with a high degree of atomic randomness and thus high bulk ionic conductivity. Additionally, the low hydroxide concentrations in the final $Li_{3-y}Ba_{y/2}OCl$ product derived from drying with a vacuum pump are expected to increase the interface conductivity.

The reasoning above is consistent with the well-known theory that the formation of amorphous and crystalline phases is a competing process with crystalline phases as stable phases and amorphous phases as metastable phases [33]. Thus, the formation of amorphous phases requires non-equilibrium conditions. This is also the case for Li_3OCl-based electrolytes. Indeed, an earlier work by Zhao and Daemen [22] has revealed that removal of water under high vacuum at the molten state of 2LiOH + LiCl mixture (at 330–360°C) can lead to formation of pure Li_3OCl without hydroxides, but Li_3OCl is crystalline rather than a mixture of amorphous and crystalline mixture. The reason for forming crystalline Li_3OCl from the molten state of 2LiOH + LiCl mixture appears to be very high reaction temperatures (at 330–360°C) which often favor the formation of equilibrium crystalline phases. Therefore, to generate amorphous Li_3OCl-based electrolytes with high ionic conductivities, the key is to create non-equilibrium synthesis conditions such as the one identified in this study, that is, hydrothermal synthesis at 250°C followed by rapid removal of OH^- and H^+ ions as steam at 250°C with the assistance of a vacuum pump.

This study is the first attempt in using vacuum to accelerate vapor releasing process in hydrothermal synthesis of amorphous Li_3OCl. The

ionic conductivity of the Ba-doped Li_3OCl synthesized with vacuum assistance is higher than that of Ba-doped Li_3OCl without vacuum assistance, as demonstrated in this study. This conclusion is also applicable when compared with other studies in the literature. For example, Ghanbari et al. [26] synthesized $Li_{2.99}Ba_{0.005}OCl$ via hydrothermal process without the assistance of a vacuum pump, and the conductivity obtained was 5.0×10^{-5} S/cm at 60 °C, lower than 7.65×10^{-3} S/cm of this study at RT.

4. Concluding remarks

In the present study, $Li_{3-y}Ba_{y/2}OCl$ solid electrolytes are synthesized via hydrothermal process and the dependance of their electrochemical properties on the hydrothermal synthesis conditions are investigated. This investigation has led to the following conclusions.

1. Amorphous $Li_{3-y}Ba_{y/2}OCl$ ($0.01 < y < 0.04$) electrolytes can be synthesized via hydrothermal process.
2. Hydrothermal reaction temperature at 250°C along with rapid removal of OH^- and H^+ ions from water-solvated $Li_{3-y}Ba_{y/2}OCl$ at 250°C, enhanced by a vacuum pump, can lead to the formation of an amorphous/crystalline $Li_{3-y}Ba_{y/2}OCl$ mixture with little hydroxide impurities because these hydrothermal synthesis and drying conditions have created a highly non-equilibrium condition for the formation of amorphous $Li_{3-y}Ba_{y/2}OCl$ electrolytes.
3. Although hydrothermal reactions and rapid removal of OH^- and H^+ ions from water-solvated $Li_{3-y}Ba_{y/2}OCl$ at 250°C without the assistance of a vacuum pump also lead to the formation of an amorphous/crystalline $Li_{3-y}Ba_{y/2}OCl$ mixture but with significant hydroxide impurities. Furthermore, the bulk conductivity of the final product is much lower than that of the amorphous/crystalline $Li_{3-y}Ba_{y/2}OCl$ mixture synthesized at 250°C followed by rapid removal of OH^- and H^+ ions from water-solvated $Li_{3-y}Ba_{y/2}OCl$ with the assistance of a vacuum pump at 250°C.
4. Hydrothermal reactions and drying at 235°C and 225°C or reactions at 250°C followed by drying at 210°C also result in amorphous/crystalline $Li_{3-y}Ba_{y/2}OCl$ mixture but with significant hydroxide impurities. The bulk conductivities of these amorphous/crystalline mixtures are lower than that of the amorphous/crystalline mixture synthesized and dried at 250°C with assistance of a vacuum pump.
5. The amorphous/crystalline $Li_{2.99}Ba_{0.005}OCl$ mixture synthesized at 250°C followed by vacuum-pump-assisted drying at 250°C has a high bulk ionic conductivity (7.65×10^{-3} S/cm) at RT, but its conductivity along grain boundaries and/or particle interfaces is low ($\sim 10^{-7}$ S/cm).
6. The amorphous/crystalline $Li_{2.99}Ba_{0.005}OCl$ mixture is stable against oxidation up to 5.3 V vs. Li^+/Li and stable against Li electrode.
7. Melting of $Li_{2.99}Ba_{0.005}OCl$ and re-solidification at a heating/cooling rate of 5 °C/min cannot promote the formation of amorphous $Li_{2.99}Ba_{0.005}OCl$.
8. The bulk conductivity of $Li_{3-y}Ba_{y/2}OCl$ increases with increasing the Ba dopant concentration, which is likely due to the increased vacancy concentration induced by the increased Ba content.
9. In contrast, the total conductivity of $Li_{3-y}Ba_{y/2}OCl$ decreases with increasing Ba dopant concentration. The possible reason for this opposite trend is the increased hydroxide impurities as Ba content increases.

CRediT authorship contribution statement

Junquan Ou: Writing – original draft, Methodology, Investigation, Formal analysis, Data curation. **Vignyatha Tatagari:** Validation, Investigation, Formal analysis, Data curation. **Ishani Senevirathna:** Methodology, Investigation, Formal analysis, Data curation. **Sudarshan Luitel:** Formal analysis, Data curation. **Carlo Segre:** Writing – review & editing, Funding acquisition, Formal analysis. **Leon Shaw:** Writing – review & editing, Supervision, Project administration, Investigation, Funding acquisition, Conceptualization. **M. Helena Braga:** Writing – review & editing, Investigation, Funding acquisition.

Declaration of competing interest

The authors of the manuscript titled "On the Formation and Properties of Amorphous and Crystalline $Li_{3-y}Ba_{y/2}OCl$ Electrolytes" declare no conflict of interest.

Data availability

Data will be made available on request.

Acknowledgements

This work was supported by the U.S. National Science Foundation (NSF) with the award numbers OISE-2230770. CS and LS are also grateful to the Duchossois Leadership Endowment Fund and the Rowe Family Endowment Fund, respectively.

Appendix A. Supplementary data

Supplementary data to this article can be found online at https://doi.org/10.1016/j.jpowsour.2024.234685.

References

[1] J. Schnell, T. Gunther, T. Knoche, C. Vieider, L. Kohler, A. Just, M. Keller, S. Passerini, G. Reinhart, All-solid-state lithium-ion and lithium metal batteries – paving the way to large-scale production, J. Power Sources 382 (2018) 160–175.
[2] A. Manthiram, X. Yu, S. Wang, Lithium battery chemistries enabled by solid-state electrolytes, Nature Reviews 2 (2017) 1–16.
[3] Z. Ding, J. Li, J. Li, C. An, Interfaces: key issue to be solved for all solid-state lithium battery technologies, J. Electrochem. Soc. 167 (2020) 070541.
[4] J. Ma, B. Chen, L. Wang, G. Cui, Progress and prospect on failure mechanisms of solid-state lithium batteries, J. Power Sources 392 (2018) 94–115.
[5] F. Mizuno, C. Yada, H. Iba, Solid-state lithium-ion batteries for electric Vehicles, in: G. Pistoia (Ed.), Li-ion Batteries – Advances and Applications, Elsevier, Oxford, 2014, pp. 273–291.
[6] W. Zhang, T. Leichtweiss, S.P. Culver, R. Koerver, D. Das, D.A. Weber, W.G. Zeier, J. Janek, The detrimental effects of carbon additives in $Li_{10}GeP_2S_{12}$-based solid-state batteries, ACS Appl. Mater. Interfaces 9 (2017) 35888–35896.
[7] R. Xu, F. Han, X. Ji, X. Fan, J. Tu, C. Wang, Interface engineering of sulfide electrolytes for all-solid-state lithium batteries, Nano Energy 53 (2018) 9538–9966.
[8] A. Sakuda, H. Kitaura, A. Hayashi, K. Tadanaga, M. Tatsumisago, Modification of interface between $LiCoO_2$ electrode and Li_2S–P_2S_5 solid electrolyte using Li_2O–SiO_2 glassy layers, J. Electrochem. Soc. 156 (2008) A27.
[9] K. Okada, N. Machida, M. Naito, T. Shigematsu, S. Ito, S. Fujiki, M. Nakano, Y. Aihara, Preparation and electrochemical properties of $LiAlO_2$-coated $Li(Ni_{1/3}Mn_{1/3}Co_{1/3})O_2$ for all-solid state batteries, Solid State Ionics 255 (2014) 120–127.
[10] S. Yubuchi, Y. Ito, T. Matsuyama, A. Hayashi, M. Tatsumisago, 5V class $LiNi_{0.5}Mn_{1.5}O_4$ positive electrode coated with Li_3PO_4 thin film for all-solid-state batteries using sulfide solid electrolyte, Solid State Ionics 285 (2016) 79–82.
[11] H.W. Kwak, Y.J. Park, Li_2MoO_4 coated Ni-rich cathode for all-solid-state batteries, Thin Solid Films 660 (2018) 625–630.
[12] Y. Seino, T. Ota, K. Takada, High rate capabilities of all-solid-state lithium secondary batteries using $Li_4Ti_5O_{12}$-coated $LiNi_{0.8}Co_{0.15}Al_{0.05}O_2$ and a sulfide-based solid electrolyte, J. Power Sources 196 (2011) 6488–6492.
[13] X. Li, J. Liu, M.N. Banis, A. Lushington, R. Li, M. Cai, X. Sun, Atomic layer deposition of solid-state electrolyte coated cathode materials with superior high voltage cycling behavior for lithium ion battery application, Energy Environ. Sci. 7 (2014) 768–778.
[14] M.H. Braga, J.A. Ferreira, V. Stockhausen, J.E. Oliveira, A. El-Azab, Novel Li_3ClO based glasses with superionic properties for lithium batteries, J. Mater. Chem. A 2 (2014) 5470–5480.
[15] M.H. Braga, A.J. Murchison, J.A. Ferreira, P. Singh, J.B. Goodenough, Glass-amorphous alkali-ion solid electrolytes and their performance in symmetrical cells, Energy Environ. Sci. 9 (2016) 948–954.
[16] M.H. Braga, N.S. Grundish, A.J. Murchison, J.B. Goodenough, Alternative strategy for a safe rechargeable battery, Energy Environ. Sci. 10 (2017) 331–336.
[17] M.H. Braga, J.A. Ferreira, A.J. Murchison, J.B. Goodenough, Electric dipoles and ionic conductivity in a Na+ glass electrolyte, J. Electrochem. Soc. 164 (2017) A207–A213.

[18] M.H. Braga, C.M. Subramaniyam, A.J. Murchison, J.B. Goodenough, Nontraditional, safe, high voltage rechargeable cells of long cycle life, J. Am. Chem. Soc. 140 (2018) 6343–6352.
[19] M.H. Braga, A.J. Murchison, J.E. Oliveira, J.B. Goodenough, Low-temperature performance of a ferroelectric glass electrolyte rechargeable cell, ACS Appl. Energy Mater. 2 (2019) 4943–4953.
[20] M.H. Braga, A.J. Murchison, J.B. Goodenough, Dataset on a ferroelectric based electrostatic and electrochemical Li-cell with a traditional cathode, Data Brief 29 (2020) 105087.
[21] M.H. Braga, A.J. Murchison, J.B. Goodenough, Dataset on a primary lithium battery cell with a ferroelectric Li-glass electrolyte and MnO_2 cathode, Data Brief 29 (2020) 105339.
[22] Y. Zhao, L.L. Daemen, Superionic conductivity in lithium-rich anti-perovskites, J. Am. Chem. Soc. 134 (2012) 15042–15047.
[23] Y. Yang, J. Han, M. DeVita, S.S. Lee, J.C. Kim, Lithium and chlorine-rich preparation of mechanochemically activated antiperovskite composites for solid-state batteries, Front. Chem. 8 (2020) 3–9.
[24] X. Lü, G. Wu, J.W. Howard, A. Chen, Y. Zhao, L.L. Daemen, Q. Jia, Li-rich anti-perovskite Li_3OCl films with enhanced ionic conductivity, Chem. Commun. 50 (2014) 11520–11522.
[25] X. Lü, J.W. Howard, A. Chen, J. Zhu, S. Li, G. Wu, P. Dowden, H. Xu, Y. Zhao, Q. Jia, Anti-perovskite Li_3OCl superionic conductor films for solid-state Li-ion batteries, Adv. Sci. 3 (2016) 1500359.
[26] A. Ghanbari, Z. Khakpour, A. Faeghinia, A. Massoudi, Investigating the amount of water on reducing $Li_x(OH)_yCl_z$ hydroxide phases in the synthesis of Li_3OCl anti-perovskite as a solid electrolyte in Li-ion batteries, Energy Sources, Part A Recovery, Util. Environ. Eff. 45 (2023) 12619–12632.
[27] S. Li, J. Zhu, Y. Wang, J.W. Howard, X. Lü, Y. Li, R.S. Kummar, L. Wang, L. L. Daemen, Y. Zhao, Reaction mechanism studies towards effective fabrication of lithium-rich anti-perovskites Li_3OX (X = Cl, Br), Solid State Ionics 284 (2016) 14–19.
[28] Z. Lu, C. Chen, Z.M. Baiyee, X. Chen, C. Niu, F. Ciucci, Defect chemistry and lithium transport in Li_3OCl anti-perovskite superionic conductors, Phys. Chem. Chem. Phys. 17 (2015) 32547–32555.
[29] J. Zheng, B. Perry, Y. Wu, Antiperovskite superionic conductors: a critical review, ACS Mater. Au 1 (2021) 92–106.
[30] A.G. Jolley, G. Cohn, G.T. Hitz, E.D. Wachsman, Improving the ionic conductivity of NASICON through aliovalent cation substitution of $Na_3Zr_2Si_2PO_{12}$, Ionics 21 (2015) 3031–3038.
[31] M. Luo, A.L. Ortiz, L. Shaw, Unraveling processing-structure-electrical conductivity relationships of $NaCrO_2$ cathodes for Na-ion batteries, J. Electrochem. Soc. 166 (2019) A3546–A3553.
[32] Y.W. Choi, C.M. Araujo, R. Lizárraga, Amorphisation-induced electrochemical stability of solid-electrolytes in Li-metal batteries: the case of Li_3ClO, J. Power Sources 521 (2022) 230916.
[33] D. Porter, K. Easterling, M. Sherif, Phase Transformation in Metals and Alloys, third ed., CRC Press, 2009.